Prompt photon production at colliders

P. Aurenche*
Fermi National Accelerator Laboratory, P.O. Box 500, Batavia, Illinois 60510

R. Baier
Fakultät für Physik, Universität Bielefeld, D-4800 Bielefeld 1, Federal Republic of Germany

M. Fontannaz
Laboratoire de Physique Théorique et Hautes Energies, Bâtiment 211, Université de Paris XI, F-91405 Orsay CEDEX, France

(Received 27 November 1989)

We discuss the uncertainties affecting the theoretical predictions for prompt-photon production at collider energies. The importance of studying the rapidity distribution at small values of the transverse momentum is emphasized as a means to probe the gluon distribution at low x.

I. INTRODUCTION

In the last few years the physics of prompt-photon reactions has undergone very impressive experimental developments. Many new sets of precise data[1-14] have been published covering a large domain of center-of-mass energy ($\sqrt{s}=20$ GeV to 1.8 TeV) as well as a wide range of transverse momentum. Of particular interest for the precise determination of parton distributions are the data with proton or antiproton beams on a proton target.[2-4] It is well known that the gluon density is not tightly constrained by the deep-inelastic-scattering (DIS) data since it enters only as a second-order effect in $F_2(x,Q)$, whereas the prompt γ spectrum in pp collisions is controlled both in normalization and shape (for a large enough lever arm in transverse momentum) by the gluon distribution.[15] Fitting both DIS data (which constrain the quark distributions and Λ) and direct-photon (DP) data one can thus obtain a precise determination of parton distributions in the nucleon.[16,17] This was recently done using fixed-target data with proton and antiproton beams and the DIS data of the Bologna-CERN-Dubna-Munich-Saclay (BCDMS) Collaboration.[18] As a value of $\chi^2 \sim 1$ per degree of freedom is obtained in the fit, this analysis also turns out to provide a quantitative test of QCD since two very different sets of data are found to be remarkably consistent with the theory.

It can be said that the single inclusive γ cross section probes the nucleon in the domain $x \sim x_T = 2p_T/\sqrt{s}$, where p_T is the transverse momentum of the photon (it should be remembered that the total momentum carried by the gluon is constrained by the sum rule, thus imposing a constraint on the gluon also in the unmeasured region). The present fixed-target data cover the region $x \geq 0.3$. Higher-energy data such as the CERN ISR or Fermilab E706 data are sensitive to values down to $x \sim 0.1$ or 0.2, while the collider data can reach values as low as $x = 10^{-2}$ for $\sqrt{s}=2$ TeV and $p_T = 10$ GeV/c, for example (unless otherwise stated we assume that the photon is produced at rapidity $y=0$ in the center of mass). In the global fit previously mentioned only fixed-target data were used to determine the parton densities. Since a simple analytic form was assumed for the gluon over the whole x range, predictions could be made for the higher-energy data, and good agreement was found with all published experimental results.[16]

We would like to discuss here the status of the theoretical calculations in the kinematical domain probed by the colliders and specifically the Fermilab Tevatron, and assess the reliability of the predictions. This study is motivated by the preliminary data from the Collider Detector at Fermilab[13] (CDF), which recently measured the γ spectrum in the range $10 < p_T < 30$ GeV/c. One of the salient features of direct γ production in the very-small-x_T region is the importance of the bremsstrahlung or anomalous γ component where the photon is produced in the debris of a hadronic jet. Although such a term appears only when calculating the higher-order terms, it nevertheless can be considered as a leading-logarithmic contribution since, as is well known, the fragmentation of a quark into a photon involves a large logarithmic term[19] which compensates the extra α_s power in the parton-parton scattering process. Being a fragmentation process, the bremsstrahlung component has a steeper p_T dependence than the lowest-order term and, in particular, it gives a very small contribution to the inclusive γ spectrum in the "low-energy" experiments (typically for $\sqrt{s} < 60$ GeV, say) which collect data at higher x_T values.

It turns out that all present collider experiments[11-13] measure isolated photons, thereby reducing the importance of the anomalous component in the observed cross section, but the problem is then to match the theoretical cuts to the experimental ones. Another ambiguity in the predictions is related to the shape of the fragmentation function of the final-state parton into a photon. Finally, the well-known freedom to choose arbitrary mass scales in the structure functions and the strong coupling con-

stant introduces a further uncertainty in the theoretical predictions. All these problems are discussed below and it will be seen that the predictions are very reliable over most of the p_T range accessible at the Tevatron, whereas at low transverse momenta the normalization of the cross section becomes somewhat more uncertain. As far as determining the gluon distribution at small x values this limitation is rather unwelcome. It will be seen, however, that if one considers the shape of the rapidity spectrum at fixed p_T, different gluons which describe adequately the low-energy data may yield rather drastically different rapidity dependences. This is related to the fact that the minimum x value probed is roughly $x \sim x_T e^{-y}$. To effectively exhibit the differences requires covering a rather large rapidity domain of 2.5 or 3 units around $y=0$ in the center of mass. It will also be shown that the y shape is not very sensitive to the various uncertainties mentioned above.

In Sec. II we recall the definition of the anomalous γ contribution and discuss in detail its main features. The cross section for producing an isolated photon is then introduced and the corresponding theoretical cuts are described. Next, we deal with the ambiguities related to the choice of scales: It is argued that the optimized approach[20–22] which was crucial to obtain a consistent picture between DIS and fixed-target DP data[16] also applies in the transverse-momentum range covered by future runs at the Tevatron. Comparison with the so-called standard scales is also given. Having defined our best estimate for the theoretical predictions, we proceed to study the sensitivity of the direct γ spectrum to different choices of parton distributions. It has been argued that charm plays an important role[23] in the production mechanism and this will be illustrated. Finally we turn to the correlation between the shape of the gluon distribution and the rapidity dependence of the spectrum at fixed p_T: This will illustrate the importance of having a detector with a large acceptance in rapidity at collider energies. Unless explicitly stated in Sec. II, we use everywhere for our predictions the value of Λ ($\Lambda_{\overline{\rm MS}}=231.5$ MeV, where $\overline{\rm MS}$ denotes the modified minimal-subtraction scheme) and the parton distributions from the best fit of Ref. 16.

Before going into a detailed discussion of the theoretical results we present in Fig. 1 the comparison of the preliminary CDF data[13] with our predictions concerning the isolated photon cross section at rapidity $y=0$. Two representative choices of factorization and renormalization scales are used: The optimized choice (solid line) and a "fixed-scale" choice (scales set equal to p_T, dashed line). One can appreciate the relative stability of the predictions under these two hypotheses. The agreement between the CERN collider data and the theory can be found in Refs. 11, 12, and 16.

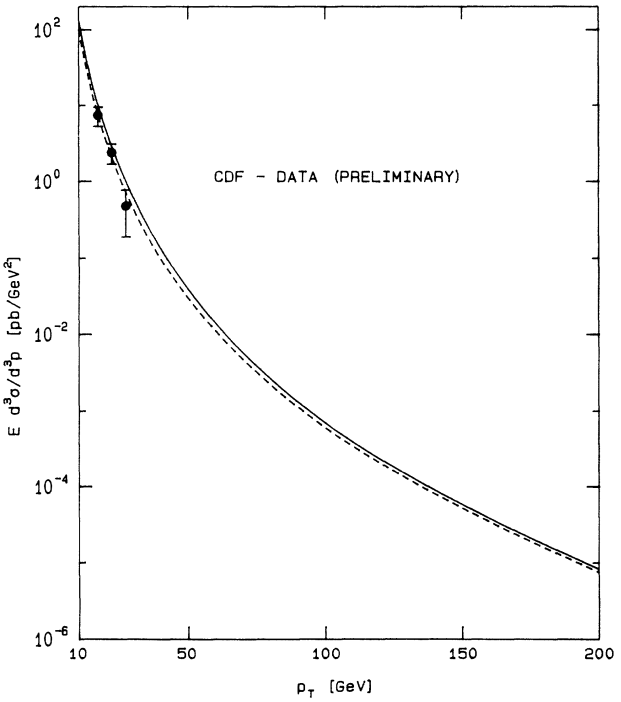

FIG. 1. Cross section for the reaction $p\bar{p}\to\gamma X$ at $\sqrt{s}=1.8$ TeV and $y=0$ as a function of p_T. The data (preliminary) are by the CDF Collaboration (Ref. 13). The curves are the QCD predictions beyond leading order as described in the text. Solid curve for optimized scales, short-dashed curve for standard scales ($\mu=M=p_T$). The CDF isolation cuts are included. The quark and gluon distribution functions are from the best fit of Ref. 16.

II. THE ANOMALOUS COMPONENT

The single-photon inclusive cross section can be written, at large transverse momentum, as

$$\frac{d\sigma}{d\mathbf{p}_T dy}=\frac{d\sigma^{\rm LO}}{d\mathbf{p}_T dy}+\frac{d\sigma^{\rm HO}}{d\mathbf{p}_T dy}+\frac{d\sigma^{\rm AN}}{d\mathbf{p}_T dy}\ , \tag{2.1}$$

where the separate terms are the leading-order, higher-order, and anomalous contributions. Details about the derivation of this equation are given in Ref. 15, where one also finds the analytic expressions for a particularly simple case, the nonsinglet case, which effectively corresponds to the difference between the $p\bar{p}$-induced and pp-induced cross sections. In the following we concentrate on a discussion of the features of Eq. (2.1) which are of special relevance to collider phenomenological studies. The various terms introduced above have the explicit form

$$\frac{d\sigma^{\rm LO}}{d\mathbf{p}_T dy}=\alpha\sum_{i,j}\int dx_1 dx_2 F_{i/\bar{p}}(x_1,M) \times F_{j/p}(x_2,M)a(\mu)\frac{d\hat{\sigma}^{ij}}{d\mathbf{p}_T dy}\ , \tag{2.2}$$

$$\frac{d\sigma^{\rm HO}}{d\mathbf{p}_T dy}=\alpha\sum_{i,j}\int dx_1 dx_2 F_{i/\bar{p}}(x_1,M) \times F_{j/p}(x_2,M)a(\mu)^2 \times r^{ij}\left[p_T,y,x_1,x_2;\frac{\mu}{p_T},\frac{M}{p_T}\right]\ , \tag{2.3}$$

$$\frac{d\sigma^{\rm AN}}{d\mathbf{p}_T dy}=\alpha\sum_{i,j}\int dx_1 dx_2 F_{i/\bar{p}}(x_1,M)F_{j/p}(x_2,M) \times a(\mu)^2\frac{d\hat{\sigma}^{ij\to q}}{d\mathbf{p}_T dy}\frac{dz}{z^2}D_{\gamma/q}(z,\hat{s})\ , \tag{2.4}$$

where i and j are the partons, in the antiproton and the proton, respectively, participating in the hard collision. The factorization scale M appears in the structure functions $F_{i/\bar{p}}(x_1,M)$ and $F_{j/p}(x_2,M)$, and the renormalization scale μ enters the couplant $a(\mu)=\alpha_s(\mu)/\pi$. All couplings have been taken out of the matrix elements and are explicitly written out. The function r_{ij} represents the higher-order corrections proper and it contains no large logarithmic terms such as $\ln(p_T^2/\Lambda^2)$ or $\ln(\hat{s}/\Lambda^2)$, where $\hat{s}$ is the parton center-of-mass energy. All such terms are collected in the anomalous contribution Eq. (2.4) which is written in such a way as to display the fragmentation mechanism which produces the photon. Note that in Eq. (2.4), there are only two independent integration variables as in Eq. (2.3), since the partonic cross section contains a δ-function constraint. The anomalous contribution arises from diagrams, such as those shown in Fig. 2, which have a pole in the invariant mass of the photon and the final-state quark.[24] Integrating over the phase space of the unobserved partons, keeping the photon momentum fixed generates the fragmentation function of the quark into a photon which has the general form

$$D_{\gamma/q}(z,\hat{s})=F_{\gamma/q}(z)\ln(\hat{s}/\Lambda^2)\ , \tag{2.5}$$

where z is the fraction of the quark momentum carried away by the photon and the splitting function $F_{\gamma/q}(z)$ is determined to be, at $O(\alpha_s^2)$ at which the calculation is carried out,

$$F_{\gamma/q}(z)=\frac{e_q^2}{2\pi}\frac{1+(1-z)^2}{z}\ . \tag{2.6}$$

The logarithmic factor in Eq. (2.5) clearly reflects the pole structure in the diagrams and the argument $\hat{s}$ is the measure of the phase space available: more precisely a factor $\hat{s}(1-z)$ is obtained in the calculation and it is purely conventional to keep only $\hat{s}$ in the definition of the anomalous component. In fact, one could have used, in Eq. (2.5), instead of $\hat{s}$ any large scale M_F^2 but terms proportional to $\ln(\hat{s}/M_F^2)$ would then appear in Eq. (2.3) so that the combination $d\sigma^{\rm AN}/d\mathbf{p}_T dy+d\sigma^{\rm HO}/d\mathbf{p}_T dy$ is independent of the choice made for the argument of the logarithm. The cutoff Λ appears naturally in QCD, but its occurrence here is, in a sense, an assumption. The best way to proceed concerning the evaluation of the anomalous component would be to determine it experimentally in a reaction such as $e^++e^-\to\gamma+X$ and use the result of the measurement in prompt-photon reactions.[25] This is similar to the method used for hadronic structure functions which are fitted in DIS experiments and the result of the fits is used to predict other cross sections. The precision of the data on photon production in e^++e^- colliders does not warrant the use of this more complicated procedure. As it stands, Λ in Eq. (2.5) should be considered as a parameter to be eventually adjusted to the prompt-photon data.

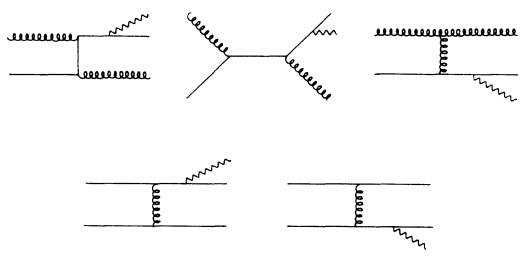

FIG. 2. Examples of diagrams contributing to the anomalous photon structure function. The wavy line represents a photon and the curly line represents a gluon.

The logarithmic factor just discussed is only one reason for the importance of the anomalous component at collider energies. The other reason is related to the partonic cross section $d\hat{\sigma}^{ij\to q}/d\mathbf{p}_T dy$. At lowest order, the parton scattering process involves a spin-$\frac{1}{2}$ exchange in the t channel, whereas the anomalous component may involve a spin-1 exchange (see Fig. 2). In the kinematical limit of interest here, namely, large $\hat{s}$ and small $\hat{t}$, the respective behavior of the cross sections is

$$\frac{d\hat{\sigma}^{ij}}{d\mathbf{p}_T dy}\simeq\frac{\hat{s}}{\hat{t}}\ , \tag{2.7}$$

$$\frac{d\hat{\sigma}^{ij\to q}}{d\mathbf{p}_T dy}\simeq\frac{\hat{s}^2}{\hat{t}^2}\ . \tag{2.8}$$

Clearly, terms such as Eq. (2.8) will dominate over Eq. (2.7) for sufficiently large $\hat{s}/\hat{t}$: This phenomenon starts to occur in the low p_T region at collider energies. It is interesting to remark that a similar situation is also encountered in the production of heavy flavors,[26] for example, charm or bottom production, at the colliders. The kinematical region probed by these processes is also such that the gluon-exchange correction diagrams dominate over the quark-exchange lowest-order terms. It has been noted[27] that this situation leads there to somewhat unstable predictions as they become quite dependent on the choice of the renormalization and factorization scales.

One can say that the lowest-order contribution and the anomalous component correspond to different topological configurations: an isolated photon in the first case and a photon in a jet in the second case. It is then reasonable to consider Eq. (2.4) as the Born term for a new production mechanism. The correction to this new term would then be similar to the corrections to the inclusive single-hadron cross section.[28] This will not be attempted here as we will see that the experimental selection criteria reduce the role of the anomalous component over most of the momentum range of interest. Also the accuracy of the experimental data does not yet justify the added complication of including these corrections.

The expression Eq. (2.6) represents the lowest-order result for the splitting function of a quark into a photon. This is phenomenologically not a very good approximation as it does not take into account the radiation of soft and collinear gluons by the quark emitting the photon. It would be akin to neglecting the scaling violations in the structure functions. It is well known that taking the gluon emission into account and summing it to all orders in the leading-logarithmic approximation modifies the z distribution of the fragmentation function Eq. (2.4) but

not the $\ln\hat{s}$ dependence. A fit to the QCD results gives[29]

$$F_{\gamma/q}(z)=\frac{1}{2\pi}\left[e_q^2\frac{2.21-1.28z+1.29z^2}{1-1.63\ln(1-z)}z^{0.049}+0.002(1-z)^2z^{-1.54}\right], \quad (2.9)$$

$$F_{\gamma/g}(z)=\frac{1}{2\pi}0.0243(1-z)z^{-0.97}. \quad (2.10)$$

The second equation arises because the gluons produced at large transverse momentum can now emit a photon, at leading order, via their breaking up into a q-$\bar{q}$ pair [$F_{\gamma/g}(z)$ obviously vanishes in the approximation where Eq. (2.6) holds]. Although Eq. (2.10) is numerically small for the z values of interest we nevertheless include it as it is well known that the $GG\to GG$ process is important in the small x_T region because both the gluon density and the matrix element are large. The fragmentation function in the leading-logarithmic approximation Eq. (2.9) falls below the lowest-order expression Eq. (2.6), and its z dependence is also steeper[29] so that it will lead to a reduction of the anomalous component. This decrease is only partially compensated by the gluon radiation process as we will see later.

Before going to the numerical illustration of the above discussion one should make some comments on the general features of the prompt γ cross section, Eq. (2.1). Based on the lowest-order contribution alone, Eq. (2.2), one finds that at $\sqrt{s}=1.8$ TeV and low-p_T values the cross section is entirely dominated by QCD Compton scattering and it is not until $p_T\sim 100$ GeV/c that the annihilation process becomes half of the Compton contribution. This illustrates the potential sensitivity to the gluon density of the prompt-photon cross section at the colliders. Of course, this statement is given only as an indication as it depends on the choice of scales. More generally, the only physical quantity is the measured cross section as the relative weights of the terms on the right-hand side of Eq. (2.1) can be modified at will by changing the scales. The full cross section, however, is more stable than its individual components. This is why in the following we will mostly show curves for the full cross section and not for its various parts separately.

We show in Fig. 3 the scaled, inclusive single-photon spectrum at $\sqrt{s}=1.8$ TeV as a function of p_T under different hypotheses. One assumes the photon is produced at rapidity $y=0$ and the factorization and renormalization scales are both set equal to p_T. The two extreme curves are obtained when setting the γ anomalous components equal to 0 (lowest curve) or when using $F_{\gamma/q}(z)$ as in Eq. (2.6) (highest curve). The two curves differ mainly at the lower end of the p_T spectrum due to the increasing role of the anomalous component in that domain. A phenomenologically more reliable prediction is obtained when using Eqs. (2.9) and (2.10). This is shown by the solid curve which illustrates the softening of the anomalous component when gluon radiation by the final-state quark is included. We have also shown the results obtained when $D_{\gamma/g}(z,\hat{s})=0$ (long-dashed line), and when comparing with the solid line one sees that, as expected, the importance of the gluon emission is confined to the small p_T region.

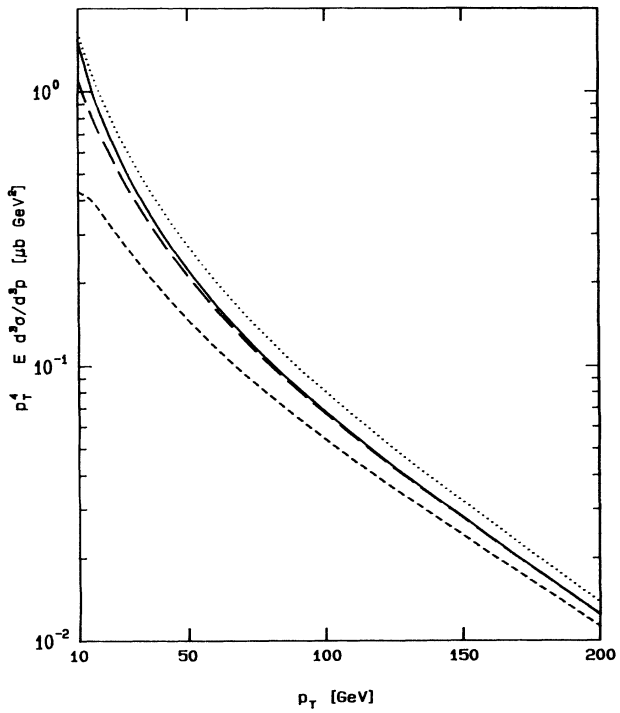

FIG. 3. The dependence of the theoretical inclusive single-photon cross section on the anomalous component. The dotted curve is obtained with the fragmentation function of Eq. (2.6) and the solid curve with the parametrization of Eqs. (2.9) and (2.10). The long-dashed curve is the result for $F_{\gamma/g}=0$, while the short-dashed one is for $F_{\gamma/q}=0$, in addition. The scales are $\mu=M=p_T$; the parameter Λ of Eq. (3.2) is taken as $\Lambda=200$ MeV.

III. THE ISOLATED-PHOTON CROSS SECTION

All collider experiments, whether at CERN or at the Tevatron, measure the inclusive cross section for an isolated photon. We discuss here how to include such a constraint in the theoretical expressions. The experimental isolation cut involves the variable

$$R=\sqrt{\Delta\eta^2+\Delta\phi^2}, \quad (3.1)$$

where $\Delta\eta$ is the pseudorapidity difference between the photon and a hadron and $\Delta\phi$ is the difference in azimuthal angles between the same. The isolation criterion is defined by $R>R_0$. We impose a similar condition but in our case it is applied to the partons which emit the photon.

As mentioned above, the logarithmic factor in the anomalous component arises because of the propagator pole in the γ-q channel which after phase-space integration gives

$$\int_{\Lambda^2/1-z}^{\hat{s}}\frac{dp^2}{p^2}=\ln\frac{\hat{s}(1-z)}{\Lambda^2}. \quad (3.2)$$

The $1-z$ factor is obtained whether one regularizes the expression by giving a mass Λ to the quark or by working

in n dimensions. Introducing an isolation cut requires carrying out the integration in Eq. (3.2) from a lower cutoff $p^2_{\min}$. In the special case where the photon is at 90° in the laboratory frame the invariant mass of the γ-q system is simply related to the angle $\delta/2$ between the γ and the quark by

$$p^2 \simeq \hat{s}(1-z)\frac{\sin^2(\delta/4)}{\cosh^2 y^*} , \tag{3.3}$$

where the collinear approximation is used to relate the parton momenta to the invariant subenergy of the hard scattering. The variable y^* is the rapidity of the center of mass of the partonic system in the laboratory: $y^*=0.5\ln x_1/x_2$. The logarithmic factor relevant to isolated-photon production is then

$$\int_{p^2_{\min}}^{\hat{s}} \frac{dp^2}{p^2} = \ln \frac{\cosh^2 y^*}{(1-z)\sin^2(\delta_0/4)} , \tag{3.4}$$

where δ_0 is the opening angle of the isolation cone around the photon. To obtain now the isolated-photon cross section one simply replaces the $\ln(\hat{s}/\Lambda^2)$ factor in the photon anomalous structure function Eq. (2.5) by $\ln[\cosh^2 y^*/(1-z)^2\sin^2(\delta_0/4)]$. It is then easy to relate the angular cut to the R_0 variable and one finds $R_0 \simeq 2\sin\delta_0/4$. We are then led to use for the anomalous component in the case of an isolated photon

$$D_{\gamma/q}(z,\hat{s}) = F_{\gamma/q}(z)\ln\frac{4\cosh^2 y^*}{(1-z)^2 R_0^2} . \tag{3.5}$$

In our derivation, we have been careful to keep factors such as $\ln(1-z)$ which can be numerically important since the effective value of z in the fragmentation process is close to 1. Without further justification a similar change is carried out in the gluon fragmentation function into a photon. One notices that "large" logarithms (e.g., $\ln\hat{s}$) do not appear and the expression for the isolated-γ cross section is now formally of $O(\alpha_s^2(\mu))$, i.e., of next-to-leading-logarithm accuracy.

In some experiments, the "isolated" photon can still be accompanied by a small amount of hadronic energy. Typically, CDF allows, for example,[13]

$$\frac{E_{\text{hadron}}}{E_\gamma} < \epsilon \tag{3.6}$$

with $\epsilon=0.15$. This energy may originate from fragments of the parton which emits the photon or from the beams. The latter contribution is small since minimum-bias hadrons have $p_T \simeq 0.45$ GeV/c with a multiplicity of five particles per unit of rapidity so that a small amount of background energy (much less than 1 GeV) should go in the region defined by $R_0 < 1$. The contribution from jet fragments can be easily estimated in the collinear approximation. Going back to the expression for the anomalous component Eq. (2.4), the phase-space boundaries, again applied at the parton level, can easily be implemented. However, it turns out that the requirement on the accompanying hadronic energy cut Eq. (3.6) gives a negligible effect when the angular cut Eq. (3.5) is already implemented. Therefore, we do not give further details here.

In the above we have discussed the bremsstrahlung contribution to the accompanied photon cross section. There are other diagrams which may contribute to this cross section. For instance, in the subprocess $G+q \to G+q+\gamma$ the gluon may fall into the cone around the photon. However, such contributions have no collinear divergences and are genuine $O(\alpha_s^2)$ corrections. Some of them may get an infrared divergence, corresponding to the gluon momentum going to 0, which is removed by the cutoff Eq. (3.6). These noncollinear contributions are expected to be small compared to the anomalous one as long as ϵ is not too close to 0. One must also keep in mind that subprocesses with a gluon exchanged in the $\hat{t}$ channel, which arise in the bremsstrahlung component [see discussion following Eq. (2.8)], become large at small p_T and at large energy compared to the processes, with a quark exchanged, that contribute to soft-gluon production.

To illustrate the importance of the angular isolation cut we show in Fig. 4 the theoretical predictions as a function of p_T for different values of R_0, namely, $R_0=0.4$, 0,7, 1, and 1.3. The cross section is normalized to the full inclusive cross section of Sec. II. The factorization and renormalization scales are chosen equal to p_T. The energy cut, Eq. (3.6), is implemented with its CDF value, but choosing $\epsilon=0$ decreases the predictions by a few percent, at most, over the whole transverse-momentum range. The z dependence of the anomalous terms is that of the leading-logarithm parametrization of Eqs. (2.9) and (2.10). Figure 4 refers to $y=0$. It clearly appears that the importance of the isolation cut is maximal at the lower p_T values.

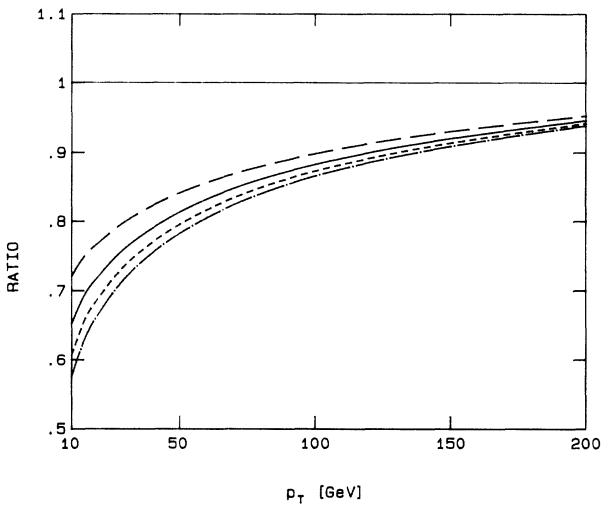

FIG. 4. The dependence of the theoretical single-photon cross section on the isolation variable R [Eq. (3.1)] as a function of p_T: $R_0=0.4$ (long-dashed curve), $R_0=0.7$ (solid), $R_0=1.0$ (short-dashed), and $R_0=1.3$ (dashed-dotted). The curves are for the ratio of the cross sections with and without the isolation cut on R, evaluated with the fragmentation functions of Eqs. (2.9) and (2.10), with fixed scales $\mu=M=p_T$.

IV. SCALE DEPENDENCE OF THE ISOLATED CROSS SECTION

In this section we consider the single isolated photon cross section, the isolation criteria being those of CDF ($R_0=0.7$, $\epsilon=0.15$) applied to the partons as described above. We use the leading-logarithmic parametrizations Eqs. (2.9) and (2.10) of the anomalous component. It is well known that calculating a cross section beyond the next-to-leading-logarithmic accuracy considerably improves the stability of the predictions: in fact, considering the lowest-order result, Eq. (2.2) in our case, alone leads to predictions which vary monotonically under changes of the renormalization or the factorization scales. On the contrary, the next-to-leading-logarithmic expression Eq. (2.1) is less sensitive to variations of the unphysical parameters since the higher-order corrections contain compensating terms.

At lower energies, it is found[22,15] that there exists a region in the (M,μ) parameter space where the cross section is stable under changes of scales (saddle-point region). Following the optimization procedure, i.e., choosing the scales in such a domain has many advantages.

(i) The predictions are not sensitive to the exact choice of scales.

(ii) The correction terms [Eqs. (2.3) and (2.4)] in the saddle-point area are small, usually less than 10%.

(iii) The approach leads to a consistent phenomenology in the sense that DIS and fixed-target DP data can be well described, with a value of $\chi^2/N_{\rm DF}\sim 1$, with a unique set of structure functions and Λ value. For four flavors it is found that $\Lambda_{\overline{\rm MS}}=231.5\pm 17$ MeV compared to $\Lambda_{\overline{\rm MS}}=209\pm 17$ MeV from the DIS data alone. The usual choice $\mu=M=p_T$ would require using a value of $\Lambda_{\overline{\rm MS}}$ in α_s between 500 and 600 MeV to obtain predictions in agreement with the DP data.

We explore in the following the effect of scale variations on the predicted cross section. We choose as our standard prediction the cross section, denoted $\sigma^{\rm opt}$, obtained by using the scales according to

$$\frac{d}{d\ln\mu}\left[\frac{d\sigma}{d\mathbf{p}_T dy}\right]=0\,,\qquad \frac{d}{d\ln M}\left[\frac{d\sigma}{d\mathbf{p}_T dy}\right]=0 \tag{4.1}$$

at $\sqrt{s}$, p_T, and y fixed. In Fig. 5 we plot the ratio

$$\frac{d\sigma}{d\mathbf{p}_T dy}(\mu=M=Cp_T)\Big/\frac{d\sigma^{\rm opt}}{d\mathbf{p}_T dy}$$

as a function of p_T, for $C=0.25$, 1, and 4. It is seen that this ratio is rather independent of C. The fixed-scale results are at most 30% lower than the optimized predictions at the smaller p_T values, a discrepancy which is less than the expected experimental errors in the foreseeable future. At larger transverse momenta ($p_T>50$ GeV/c) the spread of the results never exceeds 20%. We turn now to a more detailed discussion of the optimized predictions. We first show in Fig. 6 the variation of the isolated cross section at $p_T=20$ GeV/c with the renormalization scale μ keeping $\Lambda_{\overline{\rm MS}}$ and the factorization scale fixed (at its optimal value). We carry out the optimization procedure keeping the gluon-to-γ fragmentation function equal to 0 since no compensating terms are associated to it in $d\sigma^{\rm HO}/d\mathbf{p}_T dy$ when the scales are varied. The gluon fragmentation component is then evaluated at the optimized scales thus determined and added to the cross section. From the dotted line in Fig. 6 one can read off the range of variation of the couplant $a(\mu)$ to obtain a cross section within 15% of the optimized result. It may

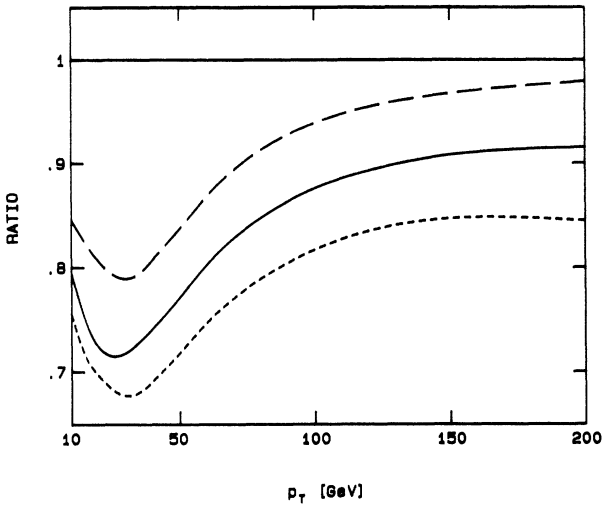

FIG. 5. The scale dependence of the inclusive single-photon production predictions in terms of the ratio of cross sections evaluated at scales $\mu=M=Cp_T$ with respect to the optimized one (isolation cuts applied). Solid curve for $C=1$, long-dashed for $C=\frac{1}{4}$, and short-dashed for $C=4$.

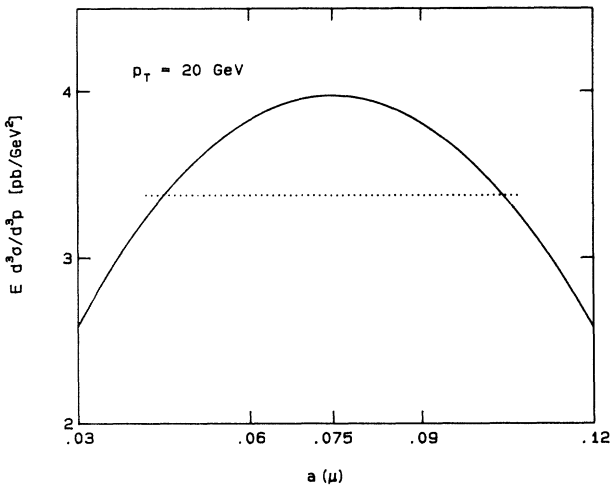

FIG. 6. Cross section at $p_T=20$ GeV as a function of the couplant $a(\mu)$ in the neighborhood of the saddle point, i.e., the factorization scale is fixed at its optimum value $M^{\rm opt}$. The solid curve is for vanishing $F_{\gamma/g}=0$. The dotted line indicates the variation from the optimum (maximal) value by 15%.

also be interesting to study the variation of $a(\mu^{\rm opt})$ as a function of p_T. This is shown in Fig. 7. The error bars on the plot define the range of variation of $a(\mu)$ around its optimal value such that the cross section varies by less than 15% from the optimized result (see the previous figure). We keep the factorization scale $M=M^{\rm opt}$ in this study. It is clear that for $p_T \geq 25$ GeV/c, the optimal coupling decreases when p_T increases, as is naively expected. Second, for a 15% accuracy on the cross section, the coupling is allowed to vary considerably. For example, at $p_T=25$ GeV/c, the permitted range for μ is 1.25 GeV $\leq \mu \leq$ 15 GeV. At smaller values of the transverse momentum the situation becomes more complex and $a(\mu^{\rm opt})$ stays constant or even decreases as p_T decreases. At the same time the values of $M^{\rm opt}$ tend to become large: $M^{\rm opt}=5p_T-20p_T$ so that the scales $\mu^{\rm opt}$ and $M^{\rm opt}$ become rather different. Such behavior can be understood when one remembers that for small p_T values one probes the small x region of the structure functions where an increase in the factorization scale increases the parton distributions, unlike what happens at larger p_T values.

In conclusion, one can say that for $p_T \geq 25$ GeV/c, the optimized results yield reasonable scales and a behavior of the coupling in accordance with the naive (i.e., neglecting kinematical constraints) expectations. For small p_T values optimization is still possible but a different pattern of scales is obtained (small μ, large M). In any case, the optimized results exceed the predictions obtained with the scales $\mu=M=p_T$ by less than 30% in the smaller p_T range and much less at higher values. In view of the phenomenological success of the optimized approach at lower energy we believe it gives the most reliable predictions, at least down to $p_T=25$ GeV/c at the Tevatron. If we turn now to the CERN collider energies we find that, for all p_T values for which data are available ($p_T \geq 13$ GeV/c), $a^{\rm opt}$ decreases as p_T increases and that the $\mu=M=p_T$ choice of scales leads to predictions which are about 30% below the optimized results at small p_T and at most 15% below at the higher transverse momenta ($p_T \geq 40$ GeV/c).

V. THE SINGLE-PHOTON SPECTRUM AS A PROBE OF PARTON DISTRIBUTIONS

It has been argued recently[23] that the charm quark in the proton would contribute a substantial amount to the photon inclusive spectrum, especially at low p_T values. Indeed at small x_T (or equivalently small x) the sea distribution dominates over the valence and, therefore, Compton scattering on the sea becomes an important component of the cross section. For the charm component to play a role one needs, furthermore, a hard enough process (here, a large enough p_T) so that its distribution can be built up, through the evolution, by the gluon splitting into $c\bar{c}$ pairs. As a way of analyzing the role played by the charm component we run the program, artificially setting the charm distribution to zero in the proton structure function, still keeping four flavors in the higher corrections and the evolution (this allows, for example, the final-state gluons to fragment into charm quark pairs). We then estimate the charm contribution by taking the difference of the full cross section with the previous estimate. We find, as expected, that the relative importance of charm increases as p_T decreases and this is independent of the choice of scales, at least down to $p_T=30$ GeV/c (Fig. 8). Below that value, the estimate becomes more scale dependent.

A question often raised about direct photon production at the colliders concerns the constraints which can be put by the data on the gluon distribution at small x. It was seen[15] that the CERN data at rapidity $y=0$ could not distinguish the "soft" Duke-Owens set-1, from the "hard" set-2 parametrization.[30] A similar study by the

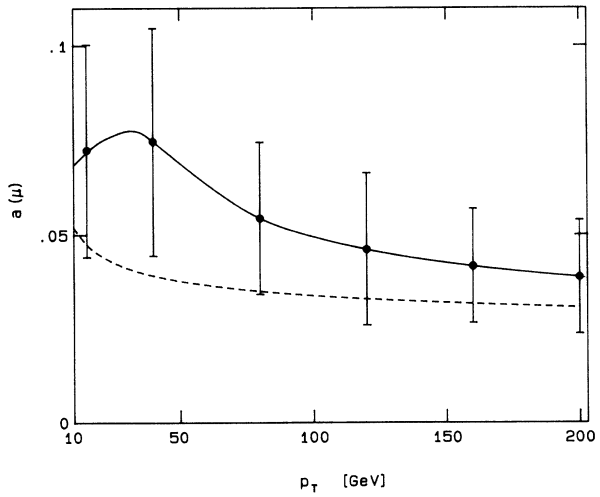

FIG. 7. The coupling constant for the "optimized" cross section as a function of p_T. The errors indicate the variation of $a(\mu)$ when a change by 15% of the cross section at its maximum value is allowed. The dashed curve is for $\mu=p_T$.

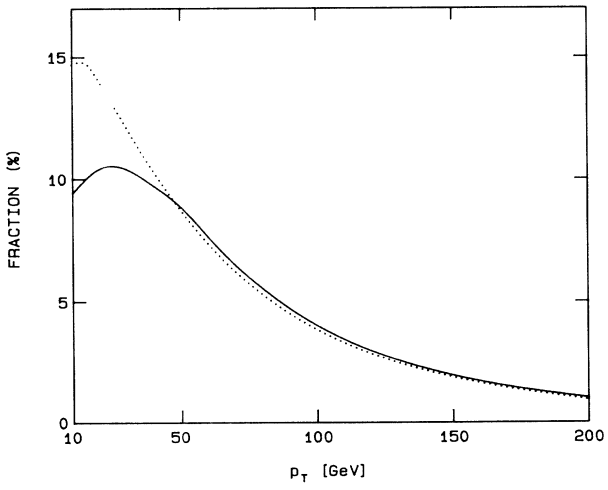

FIG. 8. Contribution of the charm content in the nucleon to the prompt-photon cross sections of Fig. 1. Solid curve for the optimized ones, dotted curve for fixed scales $\mu=M=p_T$. The number of flavors is fixed by $N_F=4$.

UA2 Collaboration[12] shows that their data did not allow to distinguish between "soft-" and "hard-" gluon distributions based on different next-to-leading-logarithmic parametrizations of the BCDMS data.[18] The essential reason for this lack of sensitivity is that the crossing point of hard- and soft-gluon distributions is in the x domain probed by these experiments. To analyze this question in more detail we consider in the following three different distributions.

(i) The gluon which gives the best fit to BCDMS and fixed-target prompt-photon data and which is parametrized as[16]

$$xG(x,Q_0^2)\simeq(1-x)^4 . \tag{5.1}$$

(ii) A soft gluon

$$xG(x,Q_0^2)\simeq(1-x)^9 , \tag{5.2}$$

in excellent agreement with the BCDMS data[18] alone which essentially probes the distribution in the range $0.07<x<0.3$ but which grossly underestimates the prompt-photon fixed-target results.

(iii) A "singular" gluon of the form

$$xG(x,Q_0^2)\simeq\frac{1}{\sqrt{x}}(1-x)^{\eta_g} , \tag{5.3}$$

following the suggestion[31] that the distribution may be rather peaked at small x. Several fits were made to the DIS data varying η_g to determine the other parameters (Λ, the valence, and the sea distributions) and it was found that for $\eta_g=2$, one could also obtain an "adequate" description of the low-energy prompt-photon data [for example, for the WA70 data one obtains $\chi^2\sim 2$ per point to be compared with $\chi^2\sim 1$ per point for the gluon distribution Eq. (5.1) when only statistical errors are used]. Even though this latter parametrization does not give the best fit to the considered experimental results, it could nevertheless be acceptable within the quoted systematic errors of the experiments. In all the above cases we take $Q_0^2=2$ GeV^2.

The resulting p_T distributions at rapidity $y=0$ (isolated cross section, optimized scales) are shown in Fig. 9. The prediction based on the singular gluon differs from the standard result essentially in the overall normalization, whereas the soft gluon gives a steeper shape. However, it would require rather precise data extending on a very large p_T range to distinguish between the various hypotheses.

Much more interesting is the study of the rapidity dis-

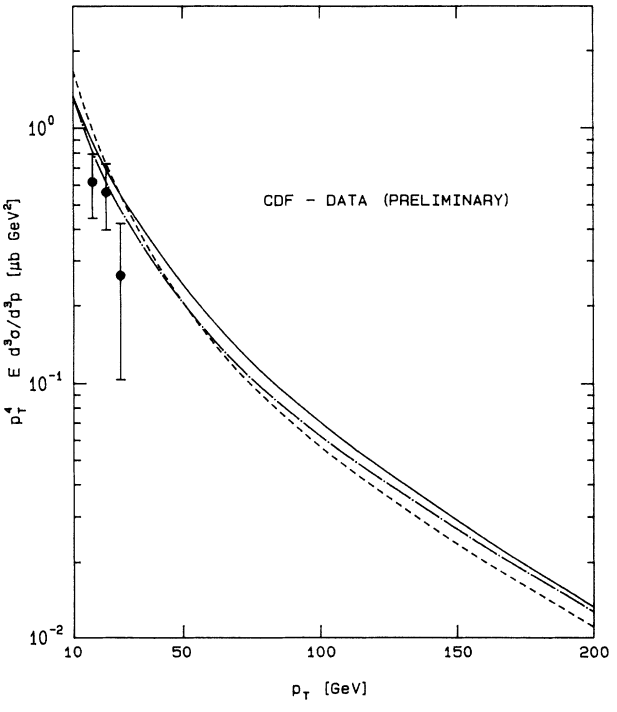

FIG. 9. Dependence of the photon cross section at $\sqrt{s}=1.8$ TeV and $y=0$ on the gluon structure function. Solid curve for the standard gluon of Eq. (5.1), dashed curve for a soft gluon [Eq. (5.2)], and dash-dotted curve for the "singular" gluon of Eq. (5.3). The cross sections are for optimized scales, and the CDF isolation cuts are included.

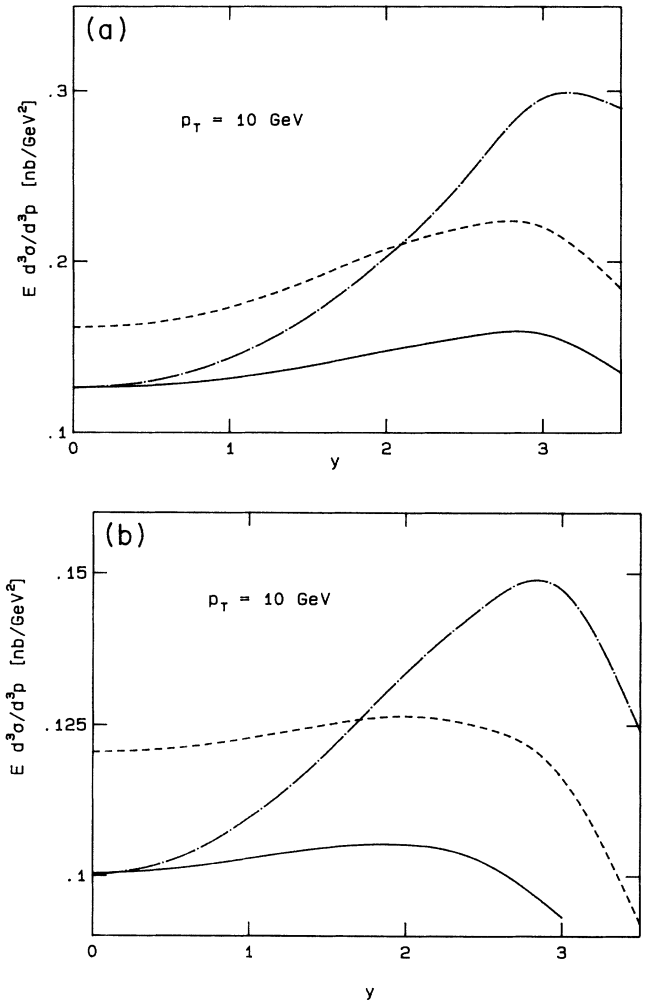

FIG. 10. (a) Dependence of the photon cross section on the gluon structure function as a function of rapidity at $p_T=10$ GeV. The curves are as in Fig. 9. (b) As above but for fixed scales $\mu=M=p_T$.

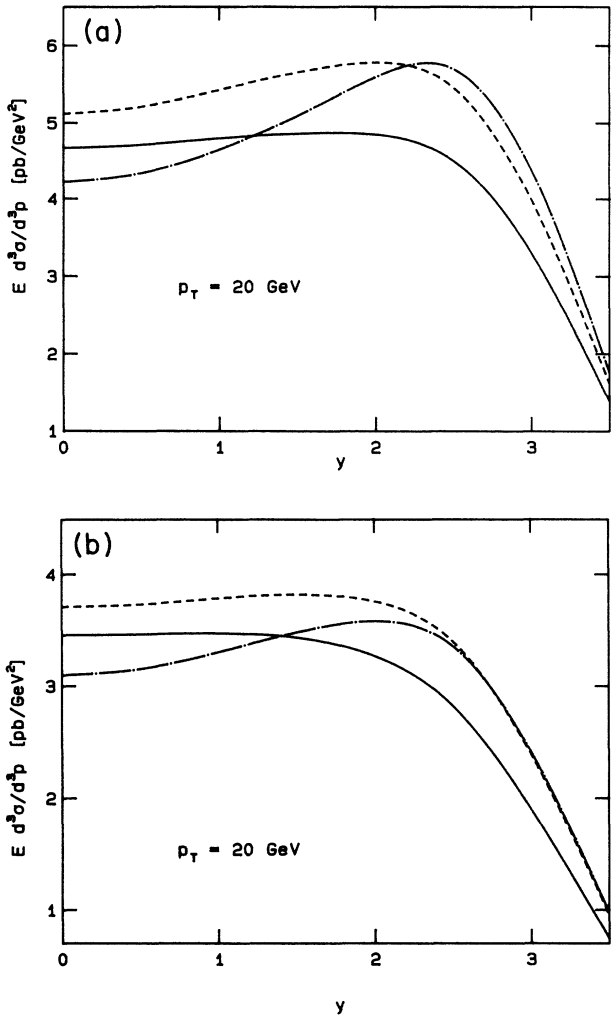

FIG. 11. As in Fig. 10, but at $p_T=20$ GeV.

tribution at small p_T values. This is shown for $p_T=10$ GeV/c on Figs. 10(a) (optimized scales) and 10(b) (scales $\mu=M=p_T$). The nonsingular gluons differ only in normalization over the whole range considered, whereas the singular gluon leads to a dramatically different shape with the cross section peaking at $y\sim 3$, and this is independent of the choices of scales. The reason for this behavior is obvious. The minimum x value probed by the inclusive distribution is

$$x_{\min}=\frac{x_T e^{-y}}{2-x_T e^{y}} \tag{5.4}$$

and larger values of the rapidity correspond to smaller values of $x_{\min}$ where the singular gluon is peaked. Unfortunately such an effect is not seen at $p_T=20$ GeV/c (Fig. 11), nor is it visible at the CERN collider energy (Fig. 12).

In conclusion, it can be said that at Tevatron energies, the rapidity distribution at low p_T values is very sensitive to a possible singular behavior of the gluon. This is a result based on the shape of a distribution and not on the

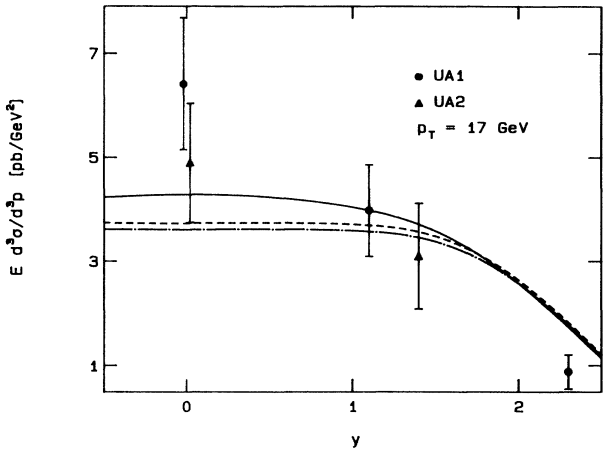

FIG. 12. Rapidity dependence of the photon cross section at $\sqrt{s}=630$ GeV and $p_T=17$ GeV for the different gluon distribution functions described in the text (see Fig. 9 for the definition of the curves). The data points are from Refs. 11 and 12 and include the systematic errors added quadratically to the statistical errors.

absolute normalization which depends somewhat on the various hypotheses entering the perturbative predictions.[32]

VI. CONCLUSIONS

In this paper we have presented a detailed study of the production of photons at large p_T in the collider energy ranges. The importance and the uncertainties of the photon anomalous (bremsstrahlung) component are stressed. Fortunately, the isolation criteria imposed by the experiments reduce the importance of this contribution so that the theoretical estimates are again of $O(\alpha_s^2)$ even though the untruncated bremsstrahlung component is formally of $O(\alpha_s)$. The theoretical uncertainties due to the choice of scales are not a problem over the whole p_T range considered. At low transverse momenta, the main uncertainties are related to the shape of the fragmentation of the partons into a photon. To obtain more precise predictions it would be necessary to implement an exclusive model[33] for this piece but care has to be taken to also include the radiation of gluons from the final-state partons; otherwise, one would overestimate this component. Such an exclusive model would also be useful to match the theoretical isolation cuts to the experimental ones more precisely. On the experimental side, it would be very interesting to collect data over a wide rapidity range at small p_T values, since the shape of the rapidity dependence of the single-photon spectrum is very sensitive to the small-x behavior of the gluon distribution.

ACKNOWLEDGMENTS

We thank A. Bamberger, R. Blair, M. Demarteau, R. K. Ellis, J. Huston, J. Qiu, H. Weerts, and M. Zielinski for discussions. One of us (R.B.) is grateful for the hospitality of Fermilab during the Summer of 1988. Partial support of this work by "Projets de Coopération et d'Echange" (PROCOPE) is gratefully acknowledged.

*Permanent address: L.A.P.P., BP 110, 74941 Annecy-le-Vieux CEDEX, France.

[1]NA3 Collaboration, J. Badier *et al.*, Z. Phys. C **31**, 341 (1986).

[2]NA24 Collaboration, C. DeMarzo *et al.*, Phys. Rev. D **36**, 8 (1987).

[3]WA70 Collaboration, M. Bonesini *et al.*, Z. Phys. C **37**, 535 (1988); **38**, 371 (1988).

[4]UA6 Collaboration, A. Bernasconi *et al.*, Phys. Lett. B **206**, 163 (1988).

[5]R108 Collaboration, A. L. S. Angelis *et al.*, Phys. Lett. **94B**, 106 (1980); Nucl. Phys. **B263**, 228 (1986).

[6]R110 Collaboration, A. L. S. Angelis *et al.*, Nucl. Phys. **B327**, 541 (1989).

[7]R806 Collaboration, E. Annassontzis *et al.*, Z. Phys. C **13**, 277 (1982).

[8]AFS Collaboration, T. Åkesson *et al.*, Report No. CERN-EP/89-98, 1989 (unpublished).

[9]E705 Collaboration, G. Zioulas, Bull. Am. Phys. Soc. **34** (1989).

[10]E706 Collaboration, J. Huston, in *Proceedings of the XIV International Symposium on Lepton and Photon Interactions,* Stanford, California, 1989, edited by M. Riordan (World Scientific, Singapore, 1990).

[11]UA1 Collaboration, C. Albajar *et al.*, Phys. Lett. B **209**, 385 (1988); **209**, 397 (1988).

[12]UA2 Collaboration, R. Ansari *et al.*, Phys. Lett. B **176**, 239 (1986); Z. Phys. C **41**, 395 (1988).

[13]CDF Collaboration, R. Blair, Argonne Report No. ANL-HEP-CP-07 (unpublished).

[14]For a compilation of data, see P. Aurenche and M. R. Whalley, Rutherford Laboratory Report Nos. RAL-89-106, DPDG/89/04, 1989 (unpublished).

[15]P. Aurenche, R. Baier, A. Douiri, M. Fontannaz, and D. Schiff, Phys. Lett. **140B**, 87 (1984); P. Aurenche, R. Baier, M. Fontannaz, and D. Schiff, Nucl. Phys. **B297**, 661 (1989).

[16]P. Aurenche, R. Baier, M. Fontannaz, J. F. Owens, and M. Werlen, Phys. Rev. D **39**, 3275 (1989).

[17]For an alternative point of view, based, however, on the higher-order calculation (including the corresponding computer code) of Ref. 15, see D. Atwood, A. P. Contogouris, and S. Papadopoulos, McGill University report, 1989 (unpublished).

[18]BCDMS Collaboration, A. C. Benvenuti *et al.*, Phys. Lett. B **223**, 485 (1989); **223**, 490 (1989).

[19]K. Koller, T. F. Walsh, and P. M. Zerwas, Z. Phys. C **2**, 197 (1979).

[20]G. Grunberg, Phys. Lett. **95B**, 70 (1980); Phys. Rev. D **29**, 2315 (1984).

[21]P. M. Stevenson, Phys. Rev. D **23**, 2916 (1981); P. M. Stevenson and H. D. Politzer, Nucl. Phys. **B277**, 758 (1986).

[22]For a detailed discussion of the use of the optimization procedure in hadronic reactions involving real photons, see P. Aurenche, R. Baier, M. Fontannaz, and D. Schiff, Nucl. Phys. **B286**, 509 (1987).

[23]R. S. Fletcher, F. Halzen, and E. Zas, Phys. Lett. B **221**, 403 (1989).

[24]E. L. Berger, E. Braaten, and R. D. Field, Nucl. Phys. **B239**, 52 (1984).

[25]P. Aurenche and J. Lindfors, Nucl. Phys. **B168**, 296 (1980).

[26]P. Nason, S. Dawson, and R. K. Ellis, Nucl. Phys. **B303**, 607 (1988).

[27]G. Altarelli, M. Diemoz, G. Martinelli, and P. Nason, Nucl. Phys. **B308**, 724 (1988).

[28]F. Aversa, P. Chiappetta, M. Greco, and J. Ph. Guillet, Phys. Lett. B **210**, 225 (1988); **211**, 465 (1988).

[29]J. F. Owens, Rev. Mod. Phys. **59**, 465 (1987).

[30]D. W. Duke and J. F. Owens, Phys. Rev. D **30**, 49 (1984).

[31]J. C. Collins, in *Supercollider Physics,* proceedings of the Workshop on Super High Energy Physics, Eugene, Oregon, 1985, edited by D. E. Soper (World Scientific, Singapore, 1986).

[32]More complete predictions concerning the role of the gluon can be found in H. Weerts, in *Physics at Fermilab in the 1990's,* proceedings of the Workshop, Breckenridge, Colorado, 1989, edited by D. Green and H. J. Lubatti (World Scientific, Singapore, in press).

[33]H. Baer, J. Ohnemus, and J. F. Owens, Phys. Lett. B **234**, 127 (1990).